

Abstract

In this article we propose a new type of optical vortex, the X-type vortex. This vortex inherits and develops the conventional noncanonical vortex, i.e., it no longer has a constant phase gradient around the center, while the intensity keeps invariant azimuthally. The strongly focusing properties of the X-type vortex and its effect on the beam shaping in three-dimensional (3D) fields are analyzed. The interesting phenomena, which cannot be seen in canonical vortices, are observed, for instance the ‘switch effect’ which shows that the intensity pattern can switch from one transverse axis to another in the focal plane by controlling the phase gradient parameter. It is shown that by adjusting the phase gradient of this vortex, the focal field can have marvelous patterns, from the doughnut shape to the shapes with different lobes, and the beam along propagation direction will form a twisting shape in 3D space with controllable rotation direction and location. The physical mechanisms underlying the rule of the beam shaping are also discussed, which generally say that the phase gradient of the X-type vortex, the orbital angular momentum, the polarization and the ‘non-generic’ characteristic contribute differently in shaping fields. This new type of vortex may supply a new freedom for tailoring 3D optical fields, and our work will pave a way for exploration of new vortices and their applications.

Keywords: optical vortex, beam shaping, structured light, singularity, 3D optical field

X-type vortex and its effect on beam shaping

Xiaoyan Pang ^{*a}, Weiwei Xiao^a, Han Zhang^a, Chen Feng^a, and
Xinying Zhao^{†b}

^{a1} School of Electronics and Information, Northwestern Polytechnical
University, Xi'an, China

^{b2} School of Physics and Information Technology, Shaanxi Normal
University, Xi'an, China

October 7, 2021

1 Introduction

Vortices, also called phase singularities, have been studied more than 30 years in optics [1, 2, 3]. Since their topological structure and carrying orbital angular momentum (OAM), optical vortices are one of the main objects of study in singular optics, and also have found numerous applications, ranging from optical tweezers [4], microscopy [5] and imaging [6], optical communications [7], to metrology [8] and astronomy[9]. Although the vortex is a natural structure and can occur generically in light fields [1, 2], the type of the vortices in most studies and applications is only the ‘canonical’ one [3], i.e. the phase gradient is constant along a circular path around the vortex center, which can be simply expressed as $Ae^{in\phi}$ (A is the field amplitude, ϕ is azimuthal angle and n denotes the topological charge). Essentially, the $2\pi n$ of phase change does not need to be distributed uniformly around the vortex center; in other words, the vortex can be ‘noncanonical’ [10]. The ‘noncanonical’ means that the phase gradient of the vortex is not constant, but the topological charge is the same as it in its ‘canonical’ counterpart [11, 12, 13].

The noncanonical vortices actually were studied by several scientists around the year 2000 [11, 12, 13, 14, 15], while only the forms of the non-canonical vortices satisfying the paraxial wave equation were taken into consideration. There, the ‘noncanonical’ vortices were also called ‘anisotropic’

*corresponding author: xypang@nwpu.edu.cn

†corresponding author: zhaoxinying@snnu.edu.cn

vortices [14, 15], since not only the phase but also the amplitude of such vortices were spatially anisotropic. Perhaps this anisotropic structure limited the study of these vortices theoretically and experimentally, so the non-canonical vortices were visited rarely in recent years [16]. In this article, we will propose a new type of noncanonical vortices which is easy to construct and its focusing properties will also be discussed.

The application/processing of laser is always accompanied by beam shaping, from reshaping the ‘elliptical’ far-field pattern into almost ‘circular’ at an early stage [17], to generating a flat-top focus [18] and multi-foci profiles [19] in a two-dimensional (2D) plane, and shaping special structures in three-dimensional (3D) fields [20, 21, 22], such as twisting beams [23], optical cages and needles [24, 25, 26], etc. The beam shaping is still an active research field that supplies various methods in inverse problems for getting desired beam patterns [21, 22, 27] and also gives rise to new research directions in study of structured light [28, 29]. There are many ways used in beam shaping, basically, including tailoring single parameter, like controlling the spatial distribution of the phase [18, 30], the polarization [20, 25], the coherence [31, 32] of the input beams, and manipulating multi-parameters, for instance the phase-coherence method [33, 34], the phase-polarization method [27], the amplitude-phase-polarization joint method [35]. Here we will show that by controlling the strength factor of the proposed noncanonical vortex, the focal pattern and the beam shape in a 3D focused fields can experience marvelous changes. That will provide a new perspective for beam shaping and may be used in many applications, such as optical tweezers [3, 4] and laser material processing [36].

A conventional noncanonical vortex embedded in a beam center can be expressed as [11, 12]

$$E(x, y) = A(x, y)(x + i\sigma_c y)^n, \quad (1)$$

with $A(x, y)$ the transverse distribution of the host beam, and the topological charge of the vortex is $\pm n$ ($n > 0$), i.e. $+n$ for $\text{Re}[\sigma_c] > 0$, and $-n$ for $\text{Re}[\sigma_c] < 0$. σ_c determining the noncanonical strength of the vortex is usually called ‘anisotropy parameter’. This equation also indicates that the topological charge of this noncanonical vortex is independent of $|\sigma_c|$ if $\text{Re}[\sigma_c] \neq 0$. When Eq. (1) is written in the polar coordinates (ρ, ϕ) ($x = \rho \cos \phi$, $y = \rho \sin \phi$) as

$$\begin{aligned} E(\rho, \phi) &= A(\rho, \phi)(\rho \cos \phi + i\sigma_c \rho \sin \phi)^n \\ &= A(\rho, \phi)\rho^n M(\phi, \sigma_c)e^{in \arctan(\sigma_c \tan \phi)}, \end{aligned} \quad (2)$$

with $M(\phi, \sigma_c) = \left(\sqrt{\cos^2 \phi + \sigma_c^2 \sin^2 \phi}\right)^n$, one can see clearly that as $|\sigma_c|$ varies, except the topological charge, both the phase and the amplitude change their distributions, which means that the field with this vortex is

‘anisotropic’ on both the phase and the amplitude. In other words, the ‘anisotropic’ distributions of the phase and amplitude are coupling in the ‘anisotropic parameter’ σ_c . That makes the noncanonical vortex not a ‘pure’ description of the helical wavefront. Thus, here we propose a new type of ‘pure’ noncanonical vortex (whose amplitude is independent of the ‘anisotropy parameter’ σ_c) named as *X-type vortex* (the reason for this name will be explained later). This X-type vortex can be expressed as

$$E^{(X)}(\rho, \phi) = A(\rho, \phi)\rho^n e^{in \arctan(\sigma_c \tan \phi)}, \quad (3)$$

which shows that σ_c only determines the phase structure (here we still adopt the convention that σ_c is named as ‘anisotropic’ parameter). When $\sigma_c = \pm 1$, this vortex becomes a ρ type canonical vortex and if $A(\rho, \phi)$ is also Gaussian Eq. (3) is actually an approximation expression of a LG beam in the transverse plane. For simplicity but without loss of generality, from here on, we assume $A(\rho, \phi) = e^{-\rho^2/w_0^2}$ (i.e. a Gaussian profile), with w_0 the beam width. This proposed X-type vortex can be generated easily through the common methods for the canonical vortex, such as by using a spatial light modulator or a spatial phase plate.

From Eq. (3), we can see that the amplitude or the intensity gradient of this vortex along the ϕ direction is zero, while the phase $\Phi = n \arctan(\sigma_c \tan \phi)$ is a nonlinear function of ϕ with its gradient calculated as

$$\nabla\Phi = \frac{d\Phi}{d\phi} = \frac{n\sigma_c}{\cos^2 \phi + \sigma_c^2 \sin^2 \phi}. \quad (4)$$

The phase and the intensity distribution of the X-type vortex are shown in Fig. 1, where the topological charge is 1 in the first two lines and is 2 in the last two lines. σ_c are selected as 0.5, 1 and 2 separately in the three columns. Then based on Eqs. (3) and (4) and Fig. 1, the properties of the X-type vortex can be summarized as follows:

- The intensity distribution is independent of σ_c , see Fig. 1 (a’)-(f’).
- $\nabla\Phi(\phi = 0) = \nabla\Phi(\phi = \pi)$ and $\nabla\Phi(\phi = \pi/2) = \nabla\Phi(\phi = -\pi/2)$. This means that the phase gradient of this vortex is symmetric about both the x -axis and the y -axis, i.e. it has a ‘cross’ (‘X’) symmetry, so this is the reason for calling this vortex as the X-type vortex [see Fig. 1 (a)-(f)].
- If $|\sigma_c| = 1$, $\nabla\Phi = \pm n$, i.e. the phase gradient is a constant. In this case, the X-type (noncanonical) vortex degenerates into a canonical vortex [see Fig. 1 (b) and (e)].
- If $|\sigma_c| < 1$, the phase gradient gets its maximum $|\nabla\Phi| = |n/\sigma_c|$ at $\phi = \pm\pi/2$, the y -axis. Also the phase changes slow near the x -axis and fast near the y -axis, i.e. the slope of the phase is steeper around the y -axis [see Fig. 1 (a) and (d)].

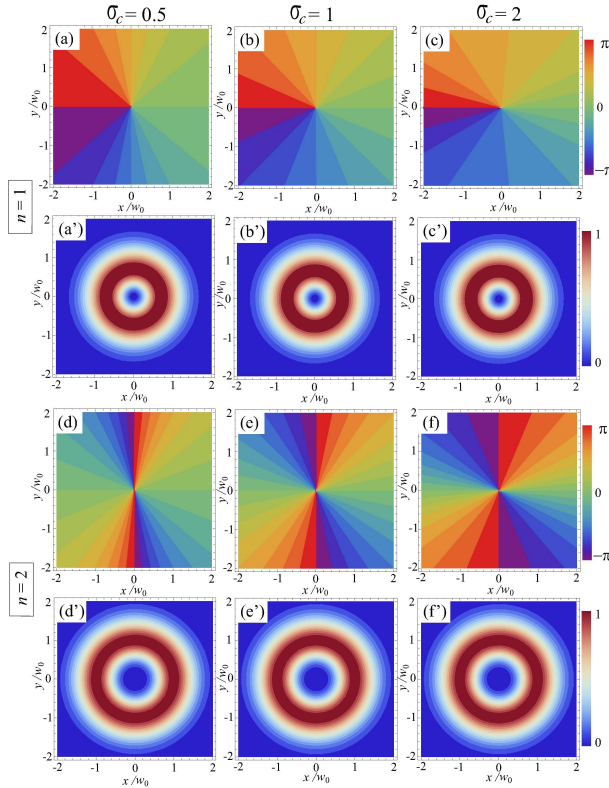


Figure 1: Color-coded plots of the phases (a)-(f) and the intensity (a')-(f') of X-type vortex. In the plots of the first two lines $n = 1$, while in the last two lines $n = 2$. $\sigma_c = 0.5, 1, 2$ for the first, second and third columns.

- If $|\sigma_c| > 1$, the phase gradient arrives at its peak $|\nabla\Phi| = |n\sigma_c|$ at $\phi = 0, \pi$, the x -axis. In this situation, the phase changes fast near the x -axis and slow near the y -axis, i.e. the slope of the phase is steeper around the x -axis [see Fig. 1 (c) and (f)].

2 Focused field

In this section we consider an aplanatic, high numerical aperture (NA) focusing system with semi-aperture angle α and focal length f , where the beam with the X-type vortex is the incident field, see Fig. 2. Assume that the incident field is linearly polarized at x direction and its complex field at the entrance plane is expressed as Eq. (3), i.e. a Gaussian type non-canonical vortex with x polarization, then according to the Richards-Wolf vectorial diffraction theory [37] the electric field \mathbf{E}^f in the focal region at an

observation point $P(\rho_s, \phi_s, z_s)$ can be expressed as

$$\begin{aligned} \mathbf{E}^f(\rho_s, \phi_s, z_s) &= \begin{bmatrix} e_x \\ e_y \\ e_z \end{bmatrix} \\ &= -\frac{ikf}{2\pi} \int_0^\alpha \int_0^{2\pi} E^X(r, \phi) \sqrt{\cos \theta} \sin \theta e^{ikz_s \cos \theta} \\ &\quad \times \begin{bmatrix} \cos \theta + \sin^2 \phi (1 - \cos \theta) \\ (\cos \theta - 1) \cos \phi \sin \phi \\ -\sin \theta \cos \phi \end{bmatrix} e^{ik\rho_s \sin \theta \cos(\phi - \phi_s)} d\phi d\theta, \end{aligned} \quad (5)$$

where k is the wave number $k = 2\pi/\lambda$ (λ is the wavelength) and (ρ_s, ϕ_s, z_s) are the cylindrical coordinates in image space ($\rho_s = \sqrt{x_s^2 + y_s^2}$). Here $E^X(r, \phi) = E^X(\rho, \phi)$ by applying the Abbe sine condition $\rho = r \sin \theta$ in the aplanatic system.

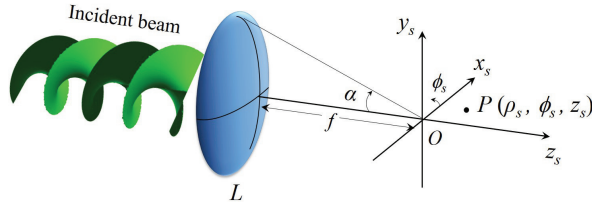


Figure 2: A strongly focusing system with a vortex beam as the incident field.

From Eq. (5), we note the following relations existing for the fields components e_x , e_y and e_z :

$$e_x^*(\rho_s, \phi_s, z_s) = -e_x(\rho_s, \pi - \phi_s, -z_s), \quad (6)$$

$$e_y^*(\rho_s, \phi_s, z_s) = +e_y(\rho_s, \pi - \phi_s, -z_s), \quad (7)$$

$$e_z^*(\rho_s, \phi_s, z_s) = -e_z(\rho_s, \pi - \phi_s, -z_s). \quad (8)$$

When $\sigma_c = 1$, i.e. the noncanonical case, besides of the relations above, the field components also satisfy:

$$e_x(\rho_s, \phi_s, z_s) = (-1)^n e_x(\rho_s, \pi + \phi_s, z_s), \quad (9)$$

$$e_y(\rho_s, \phi_s, z_s) = (-1)^n e_y(\rho_s, \pi + \phi_s, z_s), \quad (10)$$

$$e_z(\rho_s, \phi_s, z_s) = -(-1)^n e_z(\rho_s, \pi + \phi_s, z_s). \quad (11)$$

2.1 $n = 1$

In this section, we will examine the focusing properties of the first order X-type vortex ($n = 1$), and discuss its role in beam shaping.

Firstly, we will look at the field at the focal plane ($z_s = 0$). The intensity distribution of the total field is shown in Fig. 3, where σ_c is selected as 0.3 [plot (a)], 1 [plot (b)] and 3 [plot (c)], and the semi-aperture angle $\alpha = 60^\circ$. As we can see, the anisotropy parameter σ_c has a strong effect on the intensity of the field, i.e., the intensity pattern has two lobes on the x_s -axis for $\sigma_c = 0.3$, two lobes on the y_s -axis for $\sigma_c = 3$ and a (uneven) doughnut shape for $\sigma_c = 1$. In order to see this phenomenon more directly, the position variation of the intensity maxima with σ_c is drawn in Fig. 4, where the hollow marker denotes the position on x_s -axis and the solid marker denotes that on the y_s -axis. Note that since for each case there are two maxima in the focal plane and they are symmetrical about the origin, here only one of them is shown.

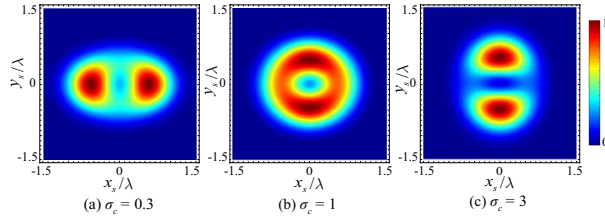


Figure 3: Intensity distribution on the focal plane: (a) $\sigma_c = 0.3$, (b) $\sigma_c = 1$, (c) $\sigma_c = 3$. In all the panels $n = 1$, $\alpha = 60^\circ$.

By analyzing Figs. 3 and 4, we can get:

- Generally, when $\sigma_c > 1$, the intensity maxima are located on the y_s -axis, while when $\sigma_c < 1$ (a little bit far from 1) the intensity maxima are on the x_s -axis, and when σ_c is near 1 (slightly < 1), the intensity will have a doughnut shape.
- There exists a switch value σ_c^{sw} , and when σ_c passes σ_c^{sw} the intensity maxima will move from x_s -axis to y_s -axis (or vice versa).
- As the semi-aperture α increases, on one hand the intensity maxima will be closer to the central axis (i.e. the distance between two intensity maxima is shorter), and on the other hand the switch value σ_c^{sw} will become smaller.

This focal shaping phenomenon physically can be explained by the joint effect of the phase gradient $\nabla\Phi$, the polarization of the incident beam and the strongly focusing. As we discussed in section 2, when $|\sigma_c| < 1$, $\nabla\Phi = 1/|\sigma_c|$ (the maximum) on the y -axis, while $\nabla\Phi = |\sigma_c|$ on the x -axis for $|\sigma_c| > 1$. This non-unit value of σ_c causes the ‘polar’ intensity distribution on these two axes (stronger on y_s for $|\sigma_c| < 1$, on x_s for $|\sigma_c| > 1$) in the far field (or in the focused field) as the beam is diffracted, and this ‘polar’

distribution will be strengthened by the high NA system. Therefore the two-lobes patterns of the intensity for $\sigma_c < 1$ and $\sigma_c > 1$ are formed [like Figs. 3 (a) and (c)]. The polarization of the incident beam is linear, x -polarization, which will lead to the intensity distributed more along the y_s -axis when the beam is strongly focused [37], and as the semi-aperture angle is larger, this anisotropic distribution becomes stronger. That is the reason for the uneven doughnut shape in the case of $\sigma_c = 1$ [Fig. 3(b)] and the smaller value of σ_c^{sw} for the larger α (see the curves for 60° and 80° in Fig. 4).

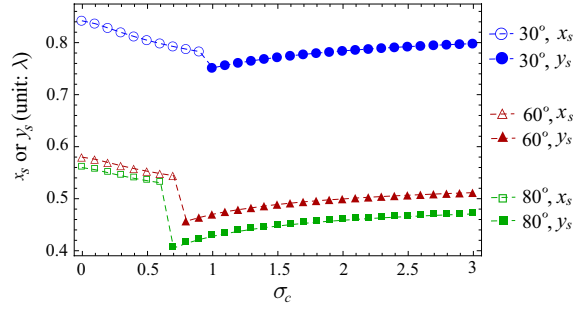


Figure 4: Locations of the intensity maxima on the focal plane with the anisotropic parameter σ_c . Here the semi-aperture angle is selected as 30° (in blue), 60° (in red) and 80° (in green).

Since the same incident intensity distribution can lead to distinguishing intensity patterns in the focal plane, there may exist intensity evolutions along the beam propagation.

Secondly, we will discuss the intensity variation with the beam propagation. Fig. 5 shows the intensity distribution on the transverse planes at $z_s = -2\lambda$, 0 and $+2\lambda$, where $\alpha = 60^\circ$ and $\sigma_c = 0.3$. We can see two intensity maxima (denoted by ‘A’ and ‘B’) still existing in different transverse planes, but they rotate with the beam propagation.

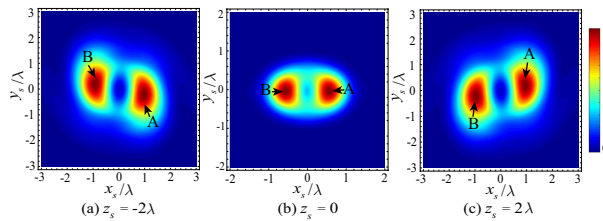


Figure 5: Intensity distribution on the transverse planes along the propagation axis. Here $\alpha = 60^\circ$, $\sigma_c = 0.3$, $n = 1$.

This rotation can be seen more straightly in Fig. 6, where the positions of the intensity maxima (points A and B, represented by red and blue spheres respectively) are drawn with z_s from -10λ to $+10\lambda$. It can be seen that

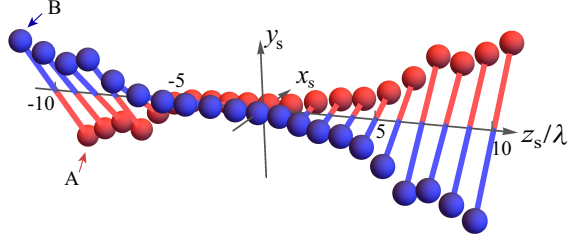


Figure 6: Positions of the two intensity maxima with z_s from -10λ to 10λ (see **Video 1**). Here $\alpha = 60^\circ$, $\sigma_c = 0.3$, $n = 1$.

the intensity maxima rotate in a counter-clockwise manner along the propagation direction. The azimuthal angle of one maximum (point A, denoted by red circles) is plotted in Fig. 7, from which we can get in the distance $-10\lambda \leq z_s \leq +10\lambda$ the maximum point rotating from about -50° to $+50^\circ$. The case for $\sigma_c = 3$ is also drawn in Fig. 7, and it shows that although there are about 90° difference between the maxima positions for $\sigma_c = 0.3$ and $\sigma_c = 3$, the maximum point for $\sigma_c = 3$ also rotates in the same manner and has the same total rotation angle as it does for $\sigma_c = 0.3$. It is also easy to illustrate that this beam rotation only occurs when $|\sigma_c| \neq 1$. Actually, the symmetry relations have implied the possibility of this rotation. From Eqs. (6)-(8), we can get

$$|e_j(\rho_s, \phi_s, z_s)| = |e_j(\rho_s, \pi - \phi_s, -z_s)|, \quad (j = x, y, z) \quad (12)$$

which means that there may exist an azimuthal rotation of the intensity distributions between the field at two sides of the origin. As we discussed before, the non-unit value of $|\sigma_c|$ ($|\sigma_c| \neq 1$) causes the ‘polar’ intensity distribution of the field when the beam passes through a lens. Thus the rotation of the beam pattern can be seen.

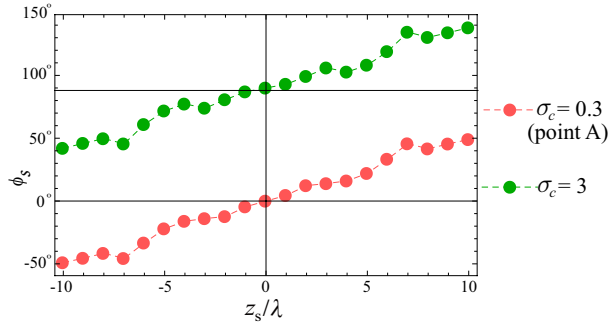


Figure 7: Azimuthal angle of the intensity maxima along the propagation direction for the incident beam of charge $+1$. Here $\alpha = 60^\circ$.

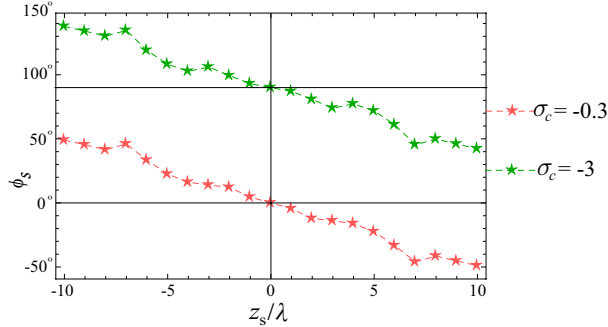


Figure 8: Azimuthal angle of the intensity maxima along the propagation direction for the incident beam of charge -1 . Here $\alpha = 60^\circ$.

This beam shaping, the rotation of the beam pattern, physically may be caused by the OAM of the noncanonical vortex. When $\sigma_c < 1$, for instance $\sigma_c = -0.3$, the topological charge of the incident beam becomes -1 , which means that the OAM has the opposite orientation of that in $\sigma_c = 0.3$. As it is shown in Fig. 8, the azimuthal angle of the maximum point for $\sigma_c = -0.3$ varies from around 50° to -50° along the propagation direction, i.e. the beam pattern rotates in a clockwise manner, which is opposite to that of $\sigma_c = 0.3$. This opposite rotation also can be seen for $\sigma_c = -3$ in Fig. 8. By comparing these two figures, Figs. 7 and 8, we can get the conclusion: for $\sigma_c > 0$, the beam pattern will rotate counter-clockwise; whereas for $\sigma_c < 0$, it will rotate clockwise. (Note that the rotation of the beam will not be observed if $|\sigma_c| = 1$.)

2.2 $n > 1$

In this section, we will consider the X-type vortex with higher topological charge, i.e. $n > 1$. The vortex with $n = 2$ and its role in the beam shaping is discussed in detail at the first two parts, then the results are generalized to other X-type vortices with higher charge.

Firstly, let us analyze the field at the focal plane for $n = 2$. The intensity distribution for different values of σ_c is shown in Fig. 9, where $\alpha = 60^\circ$. It is interesting to see that the intensity at the focal plane has ‘rich’ patterns: a two-lobe shape and a (uneven) doughnut shape (the similar patterns in $n = 1$); one bright core at center, a core with two ‘wings’ (the ‘wings’ can be spread along the x_s -axis or the y_s -axis). So there can exist one intensity maximum, two or three intensity maxima for $n = 2$. The positions of the intensity maxima with the variation of σ_c are displayed in Fig. 10, where as it is done for $n = 1$ (Fig. 4), only one maxima is drawn when there coexist two symmetric maxima. Note in this figure, the discontinues on the curves for $\alpha = 60^\circ$ and $\alpha = 80^\circ$ mean that when σ_c gets these values, the maxima

are not located at the x_s - or y_s -axis.

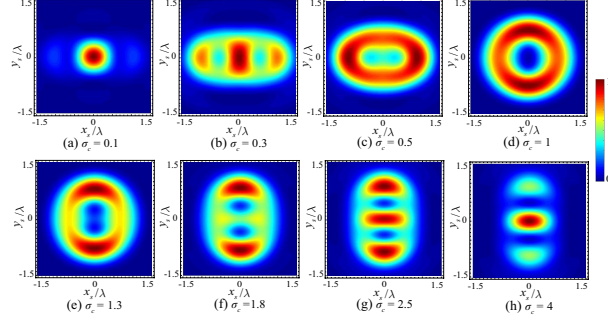


Figure 9: Intensity distribution on the focal plane: $\sigma_c = 0.1$ (a), 0.3 (b), 0.5 (c), 1 (d), 1.3 (e), 1.8 (f), 2.5 (g) and 4 (h). In all the panels $n = 2$, $\alpha = 60^\circ$.

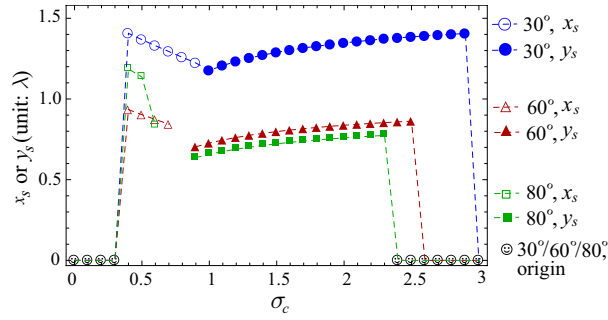


Figure 10: Locations of the intensity maxima on the focal plane with the anisotropic parameter σ_c . Here the semi-aperture angle is selected as 30° (in blue), 60° (in red) and 80° (in green), and $n = 2$.

By comparing Figs. 9,10 with Figs. 3, 4, we can get:

- Generally, the intensity maxima have a tendency to stay on the y_s -axis for $\sigma_c > 1$ and on the x_s axis for $\sigma_c < 1$, which is similar to the trend of the maxima when $n = 1$. While as σ_c goes far from 1 (like $\sigma_c = 0$ or 3), the intensity maxima will move to the origin (i.e. the position of the geometrical focus).
- The ‘switch effect’ also exists, which means that the intensity maxima will move from x_s axis to y_s axis (or vice versa) once σ_c arrives at σ_c^{sw} , however here σ_c^{sw} can be a short interval rather than one number, for instance when $\alpha = 60^\circ$, σ_c^{sw} is about $0.7 \sim 0.9$ (see the curve for 60° in Fig. 10).
- When the semi-aperture α increases, the same behavior in $n = 1$ can also be found: the intensity maxima (except those maxima locating

at the focus) are closer to the central axis and σ_c^{sw} becomes smaller, while the difference in $n = 2$ is that the maxima more likely move to the focus (i.e. the maximum goes back to the focus when $\sigma_c = 2.4$ for $\alpha = 80^\circ$, and $\sigma_c = 2.9$ for $\alpha = 30^\circ$.)

The difference appeared in the focal shaping for $n = 2$ is brought by the ‘non-generic’ characteristic of the higher order X-type vortex. When $n > 1$, the phase singularity (i.e. the vortex) in the incident vortex field is no longer fundamental, and this high order singularity will decompose into n singularities with charge ± 1 during the beam propagation according to the conservation law of the topological charge [38]. At the locations of the phase singularities, the intensity of the corresponding field component is null, thus the total intensity pattern is re-distributed.

The phase structure of the e_x component corresponding to the field in Fig. 9 is illustrated in Fig. 11, where all the parameters are the same as in Fig. 9. Here only the e_x component is chosen because it is the major component of the field and holds the initial polarization of the incident field. The singularities denoted by ‘ S_A ’ and ‘ S_B ’, evolved from the initial singularity (i.e. initial vortex with charge 2 of the incident field), play the kernel role in the intensity distribution, thus here we mainly focus on these two singularities. From Fig. 11 we can find:

- When $\sigma_c < 1$, the S_A and S_B are located symmetrically about the origin along the x_s -axis, whereas for $\sigma_c \geq 1$, their positions appear on the y_s -axis with the same symmetry relation.
- As $|\sigma_c|$ approaches 1, the distance between S_A and S_B becomes shorter.

Then, the intensity distributions in Fig. 9 can be interpreted. When $\sigma_c < 1$, although the intensity maxima distributes along the x_s -axis, since the locations of the singularities also on x_s -axis, the intensity maxima/maximum can stay at the focus [the distance between S_A and S_B is big, see Fig. 9 (a) and (b)], on x_s -axis [the distance between S_A and S_B is short, see Fig. 9 (c)]. This is also the case for $\sigma_c > 1$, and when $\sigma_c = 1.3$ [Fig. 9 (e)], the distance between S_A and S_B is short [Fig. 11 (e)] and there are two intensity maxima on y_s -axis, while as σ_c increases, the distance between S_A and S_B also increases and the intensity pattern show three lobes along y_s -axis [Fig. 9 (g)] and one bright spot at the origin [Fig. 9 (h)]. Therefore the focal shaping for $n = 2$ has been analyzed and interpreted.

Now one may raise another question: why does the vortex split into two phase singularities along the x_s -axis at the focal plane for $\sigma_c < 1$ or along the y_s -axis for $\sigma_c \geq 1$? The answer to this question will be discussed in the following part.

Secondly, we will examine the field distribution along the beam propagation. The intensity evolution for $n = 2$ along the propagation direction is

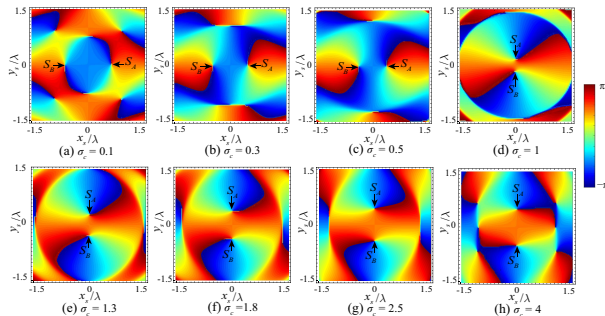


Figure 11: Phase distribution of e_x on the focal plane: $\sigma_c = 0.1$ (a), 0.3 (b), 0.5 (c), 1 (d), 1.3 (e), 1.8 (f), 2.5 (g) and 4 (h). In all the panels $n = 2$, $\alpha = 60^\circ$.

shown in Fig. 12, where $\alpha = 60^\circ$, $\sigma_c = 0.3$. One can see that the beam pattern changes from ‘two-lobe’, ‘S-shape’, ‘one-lobe’ to ‘S-shape’, ‘two-lobe’ again from $z_s = -2\lambda$ to $+2\lambda$, and at the same time the whole pattern bears a same counter-clockwise rotation as it does in the case of $n = 1$ due to the OAM of the beam. This distinguishing evolution of intensity pattern is formed mainly by the kernel singularities S_A and S_B . The phase distribution of the e_x component corresponding to the field in Fig. 12 is illustrated in Fig. 13 where S_A and S_B are marked out. It shows that these two singularities also rotate in a counter-clockwise manner, and their appearance disturbs the regular rotation behavior of the intensity distribution, thus enriches the field pattern. Actually the phase structure of the field on one side of the focus can be predicted by the phase on the other side from the symmetry relation of the focused field, Eqs. (6)-(8). According to these equations, the phase functions of e_x , e_y , e_z satisfy:

$$-\Phi_x(\rho_s, \phi_s, z_s) = \pi + \Phi_x(\rho_s, \pi - \phi_s, -z_s), \quad (13)$$

$$-\Phi_y(\rho_s, \phi_s, z_s) = \Phi_y(\rho_s, \pi - \phi_s, -z_s), \quad (14)$$

$$-\Phi_z(\rho_s, \phi_s, z_s) = \pi + \Phi_z(\rho_s, \pi - \phi_s, -z_s), \quad (15)$$

and from Eq. (13) the phase of e_x on the $-z_s$ side can be drawn from that on the $+z_s$. The symmetry relation of the phase actually also implies the rotation of the vortex.

So far we have explained the distinguishing beam shaping for $n = 2$ from the rotation behavior of the phase singularities. Now it will be of interest to get a further understanding of the propagation property of these singularities. The positions of the kernel singularities, S_A and S_B in the transverse planes with z_s from -10λ to 10λ are displayed in Fig. 14, where the orange ball and the purple ball represent the positions of S_A and S_B respectively (the parameters here are the same as in Fig. 13). From this figure, the counter-clockwise rotation is seen more directly. It also can be observed that the S_A and S_B behave more regularly than the intensity maxima for

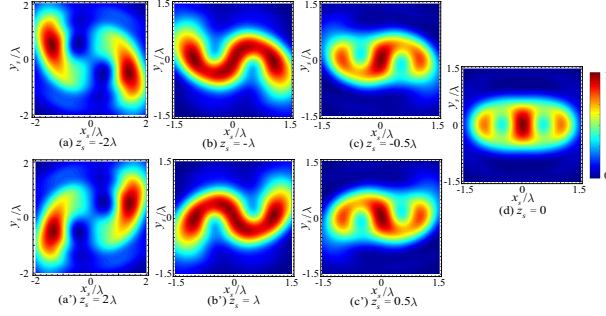


Figure 12: Intensity distribution along the beam propagation. Here $\alpha = 60^\circ$, $\sigma_c = 0.3$ and $n = 2$.

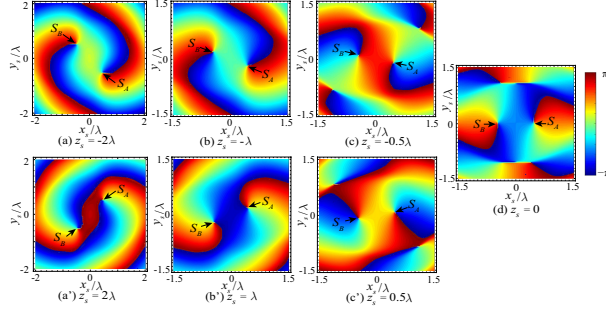


Figure 13: Phase distribution of e_x along the beam propagation. Here $\alpha = 60^\circ$, $\sigma_c = 0.3$ and $n = 2$.

$n = 2$, which is because of the topological stable of the phase singularities [1, 2]. The rotation angle of point S_A is displayed in Fig. 15, and we can see that the azimuthal angle is increased from -70° to 70° with z_s from -10λ to 10λ for $\sigma_c = 0.3$. The azimuthal angle of the vortex in the case of $\sigma_c = 3$ is also displayed and it shows that the vortex also rotates counter-clockwise from 30° to 140° . As we discussed in section 2, the rotation orientation depends on the direction of the OAM of the incident beam. In order to illustrate this point, the azimuthal rotation of the vortex for $\sigma_c < 0$ is also shown in Fig. 16, where one can see that the vortex with negative charge will rotate in a clockwise manner along the propagation direction.

Furthermore, Figs. 15 and 16, as well as Eq. (5) also indicate that if z_s goes to $-\infty$, the two vortices will be on the y_s -axis ($\phi_s = \pm 90^\circ$) for $|\sigma_c| < 1$, and on the x_s -axis ($\phi_s = 0^\circ, 180^\circ$) for $|\sigma_c| > 1$. It means that as the beam propagates from $-\infty$ to the focus the vortices rotate 90° transversely from the y_s -axis to the x_s -axis for $|\sigma_c| < 1$, whereas they rotate from the x_s -axis to the y_s -axis for $|\sigma_c| > 1$. This behavior is generated by two factors: the phase gradient of the X-type vortex and the propagation property of the

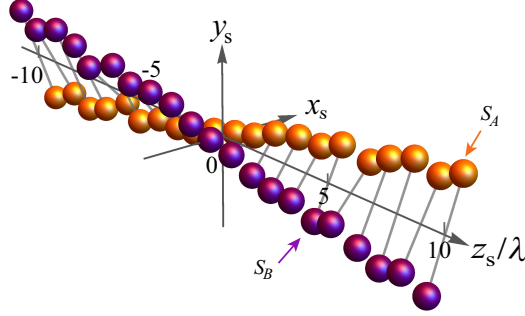


Figure 14: Positions of two vortices with z_s from -10λ to 10λ (see **Video 2**). Here $\alpha = 60^\circ$, $\sigma_c = 0.3$ and $n = 2$.

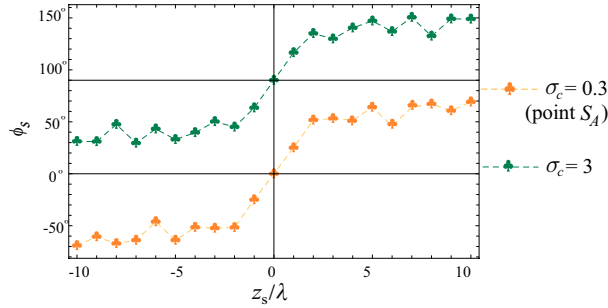


Figure 15: Azimuthal angle of the vortex along the propagation direction for the incident beam of charge $+2$. Here $\alpha = 60^\circ$.

off-axis vortex. From Eq. (4), one can get that

$$|\nabla\Phi| = \begin{cases} |n\sigma_c|, & \text{on } x\text{-axis} \\ |n/\sigma_c|, & \text{on } y\text{-axis} \end{cases} \quad (16)$$

Thus, when $|\sigma_c| < 1$, for instance $|\sigma_c| = 0.3$, $|\nabla\Phi| \approx 6.67$ on the y -axis and $|\nabla\Phi| = 0.6$ on the x -axis. Since $6.67 > 0.6$ and the ‘nongeneric’ characteristic of the higher order vortex, the vortex with topological charge ± 2 is easy to degenerate into 2 vortices along the y_s -axis as the beam passes through the lens. Similarly, if $|\sigma_c| > 1$, the vortex will split into 2 vortices located on the x_s -axis. So these two split vortices become off-axis at the ‘beginning’ of the focusing. It has been demonstrated that the off-axis vortices will experience a 90° -rotation to the focus and for the vortices with the same sign their rotation directions are the same (i.e. clockwise or counter-clockwise) [39]. Therefore, for $|\sigma_c| = 0.3$, the singularities S_A and S_B will rotate from near the y_s -axis to the x_s -axis as z_s from -10λ to 0; while for $|\sigma_c| = 3$, they rotate from near the x_s -axis to the y_s -axis. Thus the behaviors of the vortices in Figs. 15 and 16 have been explained. Then we will come to the question raised before: what is the reason for the kernel phase singularities

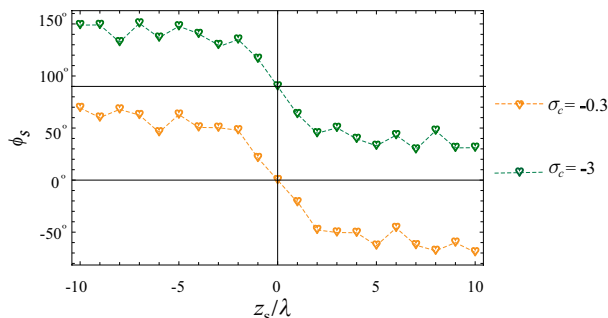


Figure 16: Azimuthal angle of the vortex along the propagation direction for the incident beam of charge -2 . Here $\alpha = 60^\circ$.

located along the x_s -axis for $\sigma_c < 1$ and along the y_s -axis for $\sigma_c \geq 1$? Now the answer is clear: because of the phase gradient of the X-type vortex and the 90° rotation of the off-axis vortex, at the focal plane the split singularities (S_A and S_B) located on the x_s -axis for $|\sigma_c| < 1$ and on the y_s -axis for $|\sigma_c| > 1$. For $|\sigma_c| = 1$, the location of S_A and S_B on y_s -axis is caused by another factor: the x -polarization of the incident beam. It is easy to demonstrate that if the beam is y -polarized at the entrance pupil, the two kernel singularities will be seen on the x_s -axis at the focal plane.

Now we can have a summary: when $n = 2$, the phase structure (i.e. the phase gradient and the topological charge) of the X-type vortex has a crucial role in the beam shaping. The rotating property of the kernel singularities, such as the rotation direction, location of the singularities and their relative distance, determines the spatial intensity patterns on both the focal plane and the 3D propagating space. In addition, at the focal plane the kernel singularities are distributed symmetrically along the x_s -axis for $|\sigma_c| < 1$, while they are along the y_s -axis symmetrically for $|\sigma_c| \geq 1$.

The above conclusion can also be generalized to any case for $n > 1$. As an example, in Fig. 17 the total intensity distribution and the corresponding phase of e_x component at the focal plane for $n = 3$ are illustrated, where the semi-aperture angle $\alpha = 60^\circ$, $\sigma_c = 0.1, 0.5, 1, 2$, and $n = 3$. As one can see, the intensity patterns can be ‘two-lobe’ along different axes, ‘four-lobe’ and ‘doughnut shaped’, which mainly depends on the locations of three kernel singularities, S_1 , S_2 and S_3 . It is also clear that S_1 , S_2 and S_3 are located along the x_s -axis for $\sigma_c = 0.1$ and 0.5 , while they have their positions on the y_s -axis for $\sigma_c = 1$ and 2 . The field distribution along the propagation direction is shown in Fig. 18, from which one can see that the three kernel singularities obey the rule summarized above: they rotate in a counter-clockwise manner along the propagation direction for $\sigma_c = 0.5$. Figs. 17 and 18 also show that the positions of the kernel phase singularities, their distance and rotation behavior shape the beam patterns at the focal plane

and in the 3D propagation space.

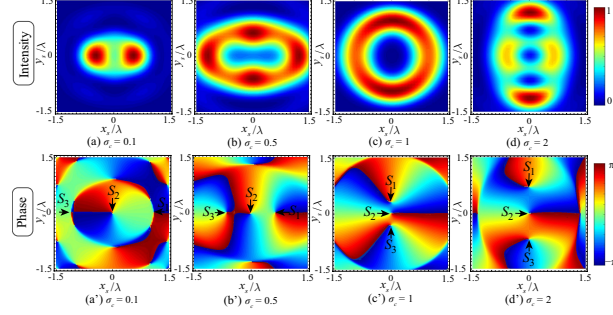


Figure 17: The field distribution at the focal plane for the X-type vortex with $n = 3$. The intensity pattern is shown in the first line, and the corresponding phase of e_x component is shown in the second line. Here $\alpha = 60^\circ$.

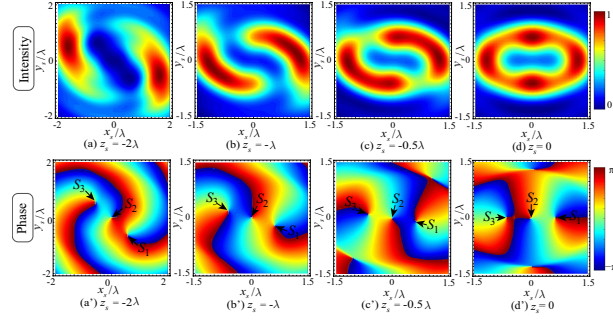


Figure 18: The field distribution with the beam propagation for the X-type vortex with $n = 3$. The intensity pattern is shown in the first line, and the corresponding phase of e_x component is shown in the second line. Here $\alpha = 60^\circ$, $\sigma_c = 0.5$.

3 Conclusions

A new type of noncanonical vortex, the X-type vortex is defined and its effects on shaping the intensity spatial distribution of a strongly focused field are discussed. We find that, firstly there exists a ‘switch effect’ of the X-type vortex, which shows that when the anisotropic parameter σ_c of the vortex passes through the switch value σ_c^{sw} ($\sigma_c^{sw} \approx \pm 1$), the intensity maxima at the focal plane will ‘switch’ from one transverse axis (for instance the x_s -axis) to another (the y_s -axis). Even a small change in σ_c near σ_c^{sw} , which may occur easily in generating a canonical vortex (i.e. $|\sigma_c| = 1$), can lead to a 90° variation in the beam pattern. This may have implications

for generation of optical vortices in experiments. Secondly, the inconstant phase gradient of the X-type vortex brings a ‘rotation’ structure of the beam in the 3D focal region, which physically is caused by the joint effect of the OAM and the anisotropic phase gradient of the vortex. This finding implies by changing the sign of σ_c (i.e. the direction of the OAM) and magnitude of σ_c can control the rotation direction and the position of the twisting strips respectively. Thirdly, when $|n| > 1$, the ‘nongeneric’ characteristic of the X-type vortex exerts a strong influence on tailoring rich field patterns in focal plane and diverse rotation strips of the beam intensity in 3D space. The physical mechanism underlying this phenomenon can be explained by the topological propagation theory of the vortices, that also suggests a new path to shape beams in 2D and 3D optical fields. Our findings offer a new vision for the fundamental properties of optical vortices, and are expected to attract further interest to applications of optical singularities.

Acknowledgement

The work was supported by National Natural Science Foundation of China (NSFC) (No. 11974281, 12104283), Natural Science Basic Research Plan in Shaanxi Province of China (No. 2020JM-116), Fundamental Research Funds for the Central Universities (No. GK202103021).

Compliance with Ethical Standards

Conflict of Interest: The authors declare that there are no conflicts of interest related to this article.

References

- [1] Soskin M S and Vasnetsov M V 2001 Singular Optics *Progress in Optics* vol 42 ed Wolf E (Elsevier) pp 219–276
- [2] Gbur G J 2017 *Singular optics* (Chemical Rubber Company)
- [3] Shen Y, Wang X, Xie Z, Min C, Fu X, Liu Q, Gong M and Yuan X 2019 *Light Sci. Appl.* **8** 90
- [4] Polimeno P, Magazzù A, Iatì M A, Patti F, Saija R, Boschi C D E, Donato M G, Gucciardi P G, Jones P H, Volpe G and Maragò O M 2018 *Journal of Quantitative Spectroscopy and Radiative Transfer* **218** 131–150
- [5] D’Ambrosio V, Spagnolo N, Del Re L, Slussarenko S, Li Y, Kwek L C, Marrucci L, Walborn S P, Aolita L and Sciarrino F 2013 *Nat. Commun.* **4** 2432

- [6] Tamburini F, Anzolin G, Umbriaco G, Bianchini A and Barbieri C 2006 *Phys. Rev. Lett.* **97** 163903
- [7] Willner A E, Huang H, Yan Y, Ren Y, Ahmed N, Xie G, Bao C, Li L, Cao Y, Zhao Z, Wang J, Lavery M P J, Tur M, Ramachandran S, Molisch A F, Ashrafi N and Ashrafi S 2015 *Adv. Opt. Photon.* **7** 66–106
- [8] Xie G, Song H, Zhao Z, Milione G, Ren Y, Liu C, Zhang R, Bao C, Li L, Wang Z, Pang K, Starodubov D, Lynn B, Tur M and Willner A E 2017 *Opt. Lett.* **42** 4482–4485
- [9] Swartzlander G A, Ford E L, Abdul-Malik R S, Close L M, Peters M A, Palacios D M and Wilson D W 2008 *Opt. Express* **16** 10200–10207
- [10] Freund I, Shvartsman N and Freilikher V 1993 *Opt. Commun.* **101** 247–264
- [11] Schechner Y Y and Shamir J 1996 *J. Opt. Soc. Am. A* **13** 967–973
- [12] Molina-Terriza G, Wright E M and Torner L 2001 *Opt. Lett.* **26** 163–165
- [13] Roux F S 2004 *J. Opt. Soc. Am. B* **21** 664–670
- [14] Freund I and Freilikher V 1997 *J. Opt. Soc. Am. A* **14** 1902–1910
- [15] Kim G H, Lee H J, Kim J U and Suk H 2003 *J. Opt. Soc. Am. B* **20** 351–359
- [16] Maji S and Brundavanam M M 2017 *Opt. Lett.* **42** 2322–2325
- [17] Braat J 1995 *Appl. Opt.* **34** 2665–2670
- [18] Nodop D, Ruecker J, Waechter S and Kahle M 2019 *Opt. Lett.* **44** 2169–2172
- [19] Guo H, Dong X, Weng X, Sui G, Yang N and Zhuang S 2011 *Opt. Lett.* **36** 2200–2202
- [20] Chen W and Zhan Q 2006 *Opt. Commun.* **265** 411–417
- [21] Chang C, Gao Y, Xia J, Nie S and Ding J 2017 *Opt. Lett.* **42** 3884–3887
- [22] Porfirev A, Ustinov A, Khonina S and Khorin P 2020 *Journal of the Optical Society of America B* **38** 420–427
- [23] Daria V R, Palima D Z and Glückstad J 2011 *Opt. Express* **19** 476–481
- [24] Weng X, Du L, Shi P and Yuan X 2017 *Opt. Express* **25** 9039–9048
- [25] Man Z, Bai Z, Li J, Zhang S, Li X, Ge X and Fu S 2018 *Appl. Opt.* **57** 3047–3055

- [26] Chen Z Y, Wei Z, Chen R and Dong J W 2021 *Opt. Express* **29** 13011–13024
- [27] Hao J, Yu Z, Hao C, Chen Z and Ding J 2014 *Appl. Opt.* **53** 785–791
- [28] Otte E, Tekce K and Denz C 2018 *Journal of Optics* **20** 105606
- [29] Forbes A, de Oliveira M and Dennis M R 2021 *Nature Photon.* **15** 253–262
- [30] Zhao X, Pang X, Zhang J and Wan G 2018 *IEEE Photon. J.* **10** 1–17
- [31] Zhao X, Pang X and Wan G 2019 *Opt. Lett.* **44** 5574–5577
- [32] Tong R, Dong Z, Chen Y, Wang F, Cai Y and Setälä T 2020 *Opt. Express* **28** 9713–9727
- [33] Xu H F, Zhang R, Sheng Z Q and Qu J 2019 *Opt. Express* **27** 23959–23969
- [34] Xu H F, Zhang R, Sheng Z Q and Qu J 2020 *Opt. Express* **28** 28858–28867
- [35] Hao J, Yu Z, Chen Z, Chen H and Ding J 2014 *Chinese Optics Letters* **12** 090501
- [36] Mhl A, Kaldun S, Kunz C, Müller F and Grf S 2019 *Journal of Laser Applications* **31** 042019
- [37] Richards B and Wolf E 1959 *Proc. R. Soc. A* **253** 358–79
- [38] Freund I and Shvartsman N 1994 *Phys. Rev. A* **50** 5164–72
- [39] Zhao X, Zhang J, Pang X and Wan G 2017 *Optics Communications* **389** 275–282 ISSN 0030-4018